Lasers in Manufacturing Conference 2023

Picosecond-pulsed laser cutting of lithium metal substrates for post-lithium-ion battery production

Johannes Kriegler[a,*], Lucas Hille[a], Michael F. Zaeh[a]

[a] *Technical University of Munich; TUM School of Engineering and Design, Department of Mechanical Engineering, Institute for Machine Tools and Industrial Management (iwb), Boltzmannstrasse 15, 85748 Garching, Germany*

Abstract

The battery industry is targeting the usage of lithium metal anodes in next-generation battery types due to their more than tenfold energy density compared to the currently dominating graphite anodes. This work explores ultrashort-pulsed laser cutting for shaping lithium metal foils to defined anode geometries. An encapsulated process environment, including a picosecond laser system, was developed, allowing the highly reactive lithium metal to be processed in an argon atmosphere. Process studies were performed, focusing on characterizing the process behavior for laser cutting of freestanding lithium metal foils and lithium metal / copper double-layers. The influence of the pulse fluence, the pulse repetition rate, and the pulse overlap on the cut edge quality was evaluated using confocal laser scanning microscopy, scanning electron microscopy, and energy-dispersive X-ray spectroscopy. The results support the design of laser cutting processes for post-lithium-ion battery production on an academic and industrial scale by comparing various processing strategies.

Keywords: laser cutting; picosecond; battery production; lithium metal

1. Introduction

Since its commercialization, lithium-ion batteries (LIB) have become the dominating electrochemical energy storage solution, particularly for electric vehicles (Blomgren 2017). Many of their appealing performance characteristics, such as excellent cycling stability and high safety, fundamentally build on the intercalation mechanism. Thereby, lithium ions shuttle between host materials, serving for lithium-ion

* Corresponding author. Tel.: +49-089-289-15531; fax: +49-089-289-15555.
E-mail address: Johannes.Kriegler@iwb.tum.de

storage (Tarascon and Armand 2001). In the most common cell design, a graphite negative electrode and a metal oxide positive electrode serve as a platform for lithium storage. However, these host materials restrict the battery´s achievable energy content and place upper physicochemical limits on energy density and specific energy (Janek and Zeier 2016).

Thus, in post-lithium-ion battery technologies, such as all-solid-state batteries (ASSBs), lithium-sulfur batteries (LSB), or lithium-air batteries (LAB), replacing graphite with pure lithium metal is targeted on the anode side (Cano et al. 2018; Placke et al. 2017; Varzi et al. 2020). Lithium metal possesses a theoretical specific capacity of ≈ 3862 mAh·g^{-1}, surpassing that of graphite with ≈ 355 mAh·g^{-1} more than tenfold (Andre et al. 2017). Due to the resulting higher specific energy and energy density at the material level (Andre et al. 2017), lithium metal anodes are thinner and lighter than graphite anodes for a given areal capacity, with target thicknesses of ≤ 20 µm (Fig. 1). In contrast, the thicknesses of conventional graphite anodes range between 50 µm and 150 µm (Duffner et al. 2021; Schmuch et al. 2018).

While lithium metal batteries have been extensively researched at the laboratory scale, their commercial success is still hindered by fundamental electrochemical challenges, such as a low Coulombic efficiency (Genovese et al. 2018) and lithium dendrite formation (Wu et al. 2018). Moreover, lithium metal is difficult to process due to its high adhesion (Meyer 1957), low Mohs hardness of 0.6 (Garrett 2004), flammability, and reactivity (Jeppson et al. 1978; Tarascon 2010). In laboratory battery manufacturing, these issues are addressed through careful manual processing (Wu et al. 2019). For instance, discrete electrodes are separated from lithium metal coils using scissors or hand punches, requiring cleaning after each operation to avoid progressive blade contamination. The resulting cut edge quality is usually not controlled and commonly accepted quality metrics are unknown. However, the efficient industrial production of lithium metal batteries with consistent performance characteristics requires scalable production processes that deliver reproducible, high-quality output.

Laser cutting is an established manufacturing technique for separating electrodes in LIB fabrication (Baumann et al. 2019; Demir and Previtali 2014; Kriegler et al. 2021). Due to the adhesive nature of lithium, the non-contact working principle of laser cutting provides an advantage over mechanical separation procedures (Duffner et al. 2021). Contact-based cutting methods require elaborate tool cleaning (Jansen et al. 2018), special blade coatings (Weber 2019), or sacrificial interlayers (Backlund 1977) to prevent tool contamination, resulting in continuous degradation of cut edge quality.

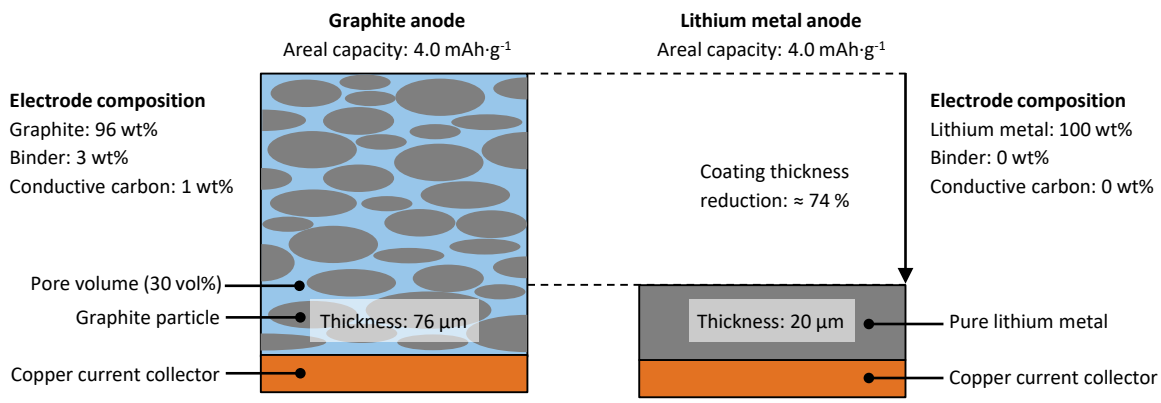

Fig. 1. Comparison of a graphite anode and a lithium metal anode with an areal capacity of 4.0 mAh·cm^{-2}; the composition and the porosity for the graphite anode were selected according to the current state-of-the-art and served as a basis for calculating the thickness of a lithium metal anode with a comparable areal capacity. Specific capacities of 355 mAh·g^{-1} and 3.862 mAh·g^{-1} were assumed for graphite and lithium metal, respectively. The thickness refers to the anode layer without a current collector.

Lithium metal is highly reactive with atmospheric gases, such as N_2, O_2, H_20, and CO_2, forming passivating layers of Li_2CO_3, LiOH, Li_2O, Li_2C_2, and LiN (Ismail et al. 2001; Otto et al. 2021; Schmitz et al. 2012). Although the safe nanosecond-pulsed laser processing of lithium metal has been demonstrated in a dry room atmosphere (dew point: ≈ -30 °C), its spontaneous ignition during laser cutting due to surface contamination raises safety concerns (Jansen et al. 2018). Furthermore, depending on the surrounding atmosphere, the thermal impact during laser cutting might accelerate surface layer formation, thus degrading the electrochemical performance of lithium metal anodes. Therefore, lithium metal processing in an inert gas atmosphere, most commonly argon, is favored (Schnell et al. 2018).

The present study aims to investigate the interaction of ultrashort-pulsed laser radiation with lithium metal substrates while providing recommendations for the industrial production of lithium metal batteries and complements the state of the art on lithium metal laser cutting (Jansen et al. 2018; Kriegler et al. 2022; Park and Lee 2021) in the following aspects:

- The laser processing of a freestanding lithium metal substrate and a lithium metal / copper double-layer with exceptionally low lithium thicknesses of ≈ 20 µm is described.
- In contrast to other investigations performed in dehumidified air in a dry room (Jansen et al. 2018) or encapsulated processing chambers (Kriegler et al. 2022; Park and Lee 2021), the experiments were conducted in an argon atmosphere by integrating a laser system into a glovebox environment suitable for the manufacture of lithium metal batteries.
- While the application of ultrashort-pulsed laser radiation was already proposed for laser cutting of conventional graphite anodes (Kriegler et al. 2021; Zhang et al. 2019), current studies on separating lithium metal foils are limited to nanosecond pulse durations (Jansen et al. 2018; Kriegler et al. 2022).

In summary, this study extends the state of the art by examining the underlying effects of material removal for various lithium metal substrates by picosecond-pulsed laser radiation.

2. Experimental approach

2.1. Materials

Two battery-grade lithium metal substrates from the same manufacturer (China Energy Lithium, China) were used for the experiments. On the one hand, a freestanding lithium metal foil with a thickness of 20 µm was processed. On the other hand, laser cutting of a double-layer composed of a 10 µm thick copper current collector and a lithium metal coating with a thickness of 20 µm was studied. The substrates were received in steel drums and individually sealed in pouch bags containing an argon atmosphere from the manufacturer. The substrates were unpacked and stored in an argon-filled glovebox (C_{H2O} < 10 ppm, C_{O2} < 1 ppm) to reduce lithium metal reaction with atmospheric constituents.

2.2. Laser system

A picosecond-pulsed laser beam source (YLPP-100-3-100-R, IPG Photonics, USA) operating at a wavelength of λ = 1030 nm was used for cutting the lithium metal substrates. Since the laser source was mounted at ambient air, the laser beam was deflected into a glovebox through an optical window via reflecting mirrors to allow laser processing under an argon atmosphere (Fig. 2 a). The raw beam diameter was enlarged before entering the galvanometric scan head (Superscan IV-15, Raylase, Germany) by introducing a beam expander into the optical path. The laser beam was focused by a fused-silica telecentric f-theta lens (JENar™ 160-1030…1080-110, Jenoptik Optical Systems, Germany) to a beam radius w_0 of 15 µm in the working plane. The parameters of the laser system are summarized in Fig. 2 b.

(a)

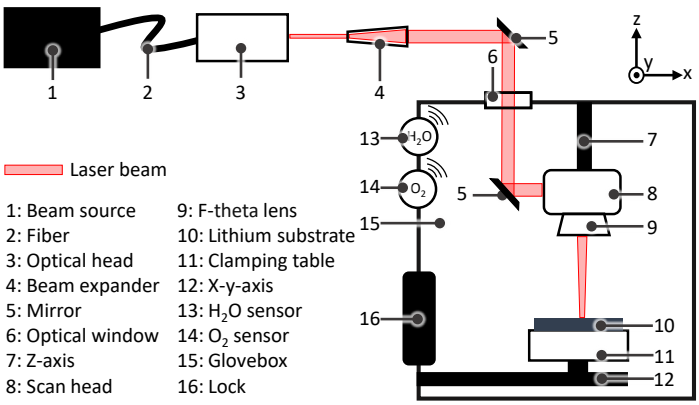

(b)

Parameter	Unit	Value
Wavelength λ	nm	1030
Pulse repetition rate f	kHz	1003, 1838, 2758
Max. pulse energy E_P	µJ	100 @ f = 1003 kHz 54 @ f = 1838 kHz 36 @ f = 2858 kHz
Pulse duration τ	ps	2
Average power P	W	< 100
Focus radius w_0	µm	15

Fig. 2. (a) Experimental setup for laser cutting of lithium metal substrates and (b) specifications of the laser system

2.3. Experimental plan

Each of the three available pulse repetition rates f was combined with five equally distributed pulse energy levels from 20 % to 100 % of the maximum available pulse energy E_p at the respective pulse repetition rate resulting in various average laser powers P. Thus, according to

$$P = E_p \cdot f, \tag{1}$$

the entire power range of the laser beam source was exploited for every pulse repetition rate. Scanning speeds v of up to 4.4 m·s^{-1} for the freestanding lithium metal foil and up to 1.8 m·s^{-1} for the lithium metal / copper substrate were applied, resulting in various pulse overlaps

$$PO = \left(1 - \frac{v}{2w_o f}\right) \cdot 100\% \tag{2}$$

for the given focus radius w_0. Instead of the pulse energy E_p, the peak pulse fluence F_0 is used as a metric within the figures to facilitate transferability of the results to other studies:

$$F_0 = \frac{2 \cdot E_p}{\pi \cdot w_0^2} \tag{3}$$

2.4. Analytics

An air-tight container was used for transporting the processed lithium metal samples from the glovebox to a dry room with a dew point of < -40 °C to analyze the cut edges. The substrate surfaces were qualitatively evaluated by a scanning electron microscope (SEM) (JSM-IT200, JEOL, Germany). Additionally, elemental analyses were performed using the SEM´s energy-dispersive X-ray spectroscopy (EDX) module. 3D laser scanning confocal microscopy (LSM) (VK-X 1000, Keyence, Japan) was used to obtain topographic information of the workpiece surface.

The generated images were tilt-corrected and analyzed with the corresponding software (MultiFileAnalyzer, Keyence, Japan). Based on visual inspection as well as on LSM and SEM images, the laser cuts resulting from different parameter sets were classified into quality classes to obtain process windows. For quantitatively analyzing the cutting kerfs, 300 equally-spaced profile lines with a distance of 0.7 µm were distributed over the microscope image perpendicular to the cutting kerf to obtain average profile lines. The average width and height of the melt superelevation along the cutting edge caused by melt displacement were measured on both sides of the kerf relative to the reference plane by determining the average values of all profile lines.

3. Results

3.1. Freestanding lithium metal foil

For the freestanding lithium metal substrate, a parameter set was defined as uncut, if no continuous cutting kerf was formed and the lithium metal was either not completely removed or only perforated (compare Fig. *3*). Successful cuts showed a distinct melt superelevation along the cut edge which was homogeneous at higher pulse repetition rates and wavy at lower pulse repetition rates. Excessive heat accumulation, especially at low scanning speeds, resulted in severely destroyed or deformed samples, impeding microscopic analysis. The average laser power resulting from the combination of pulse repetition rate and the peak pulse fluence dominated the achievable cutting speed rather than the individual values for f and F_0, respectively. Thus, high cutting speeds of ≥ 4.2 m·s^{-1} were achieved for all pulse repetition rates tested. The largest process window resulted for f = 1838 kHz, suggesting that this laser setting allows the most efficient combinations of peak pulse fluence and pulse repetition rate, balancing heat accumulation and shielding effects (Mustafa et al. 2020).

For the successful cuts, the width and height of the melt superelevation formed along the cut edges were examined to characterize the process behavior and to allow conclusions about the cut edge quality. From a quality perspective, the microstructural surface inhomogeneities are suspected to cause non-uniform lithium plating and stripping during the operation of lithium metal batteries as a consequence of an inhomogeneous current distribution (Krauskopf et al. 2020). Increasing the cutting speed resulted in less pronounced melt formation, accounting for the reduced energy input per unit length. The lowest melt width and melt heights were around 20 µm and 10 µm, respectively. These values are close to literature values achieved using nanosecond laser pulses for laser cutting a 50 µm thick freestanding lithium metal foil (Kriegler et al. 2022). Since the influence of the peak pulse fluence on the melt superelevation was rather low, but beneficial for the cutting efficiency, high peak pulse fluences in combination with high cutting speeds are to be preferred.

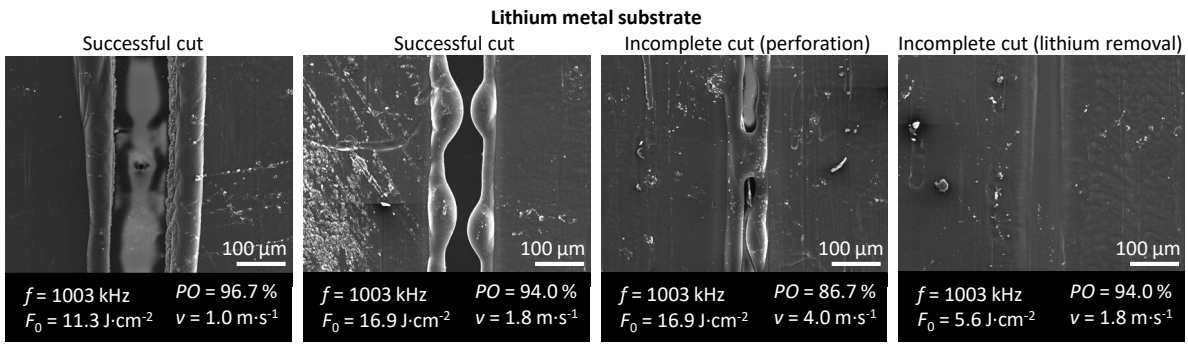

Fig. 3. Scanning electron microscopy images showing successful and incomplete laser cuts in pure lithium metal substrates; f: pulse repetition rate; PO: pulse overlap; F_0: peak pulse fluence, v: scanning speed

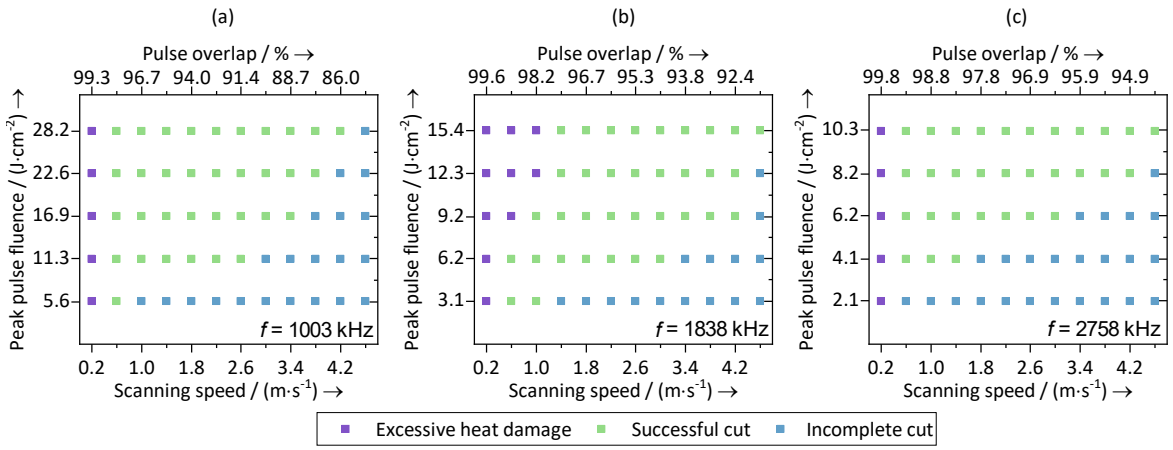

Fig. 4. Parameter windows for laser cutting of a freestanding lithium metal foil at (a) f = 1003 kHz, (b) f = 1838 kHz, and (c) f = 2758 kHz

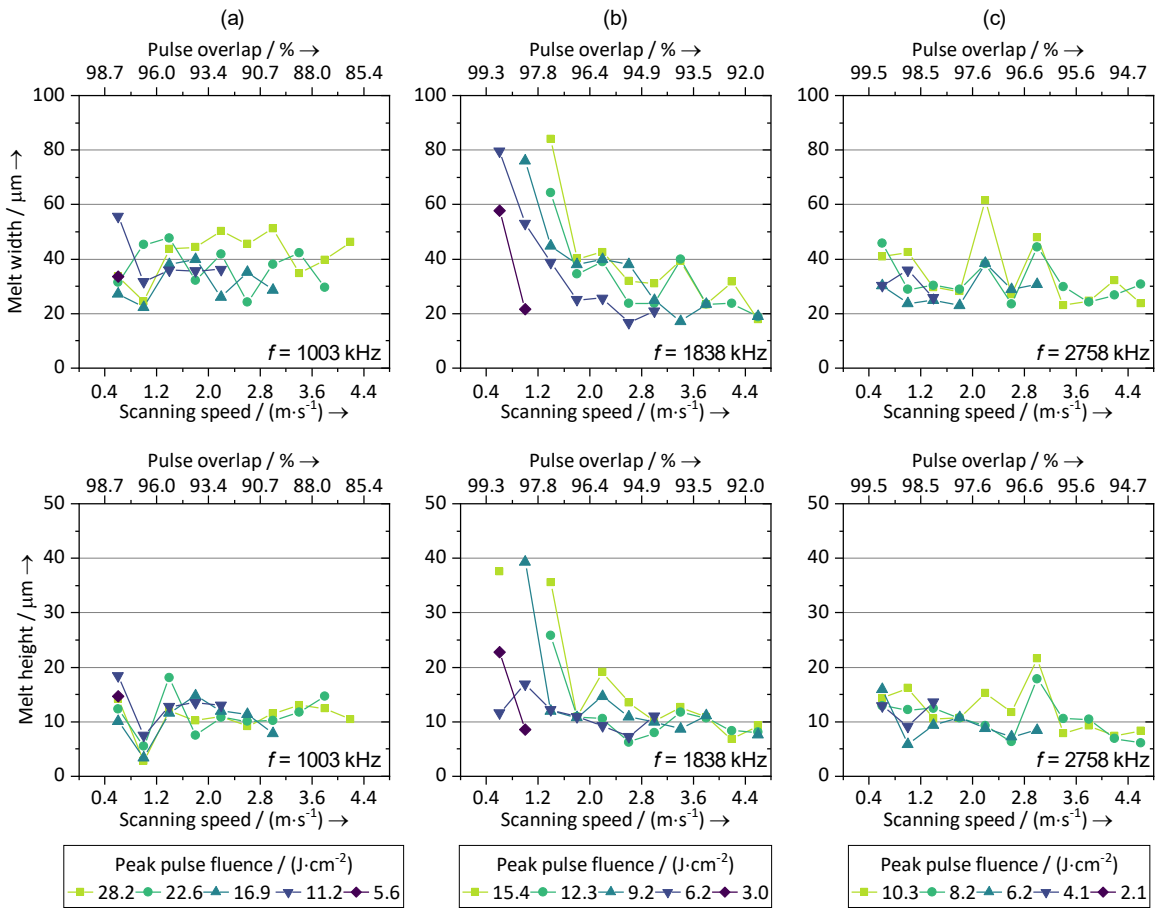

Fig. 5. Width and height of the melt superelevation of successful cuts for (a) f = 1003 kHz, (b) f = 1838 kHz, and (c) f = 2758 kHz

Despite the application of picosecond laser pulses, the material removal mechanism was mainly based on melt expulsion. Thus, a distinct melt superelevation formed along the cut edges, resulting in a material removal behavior comparable to nanosecond laser cutting of lithium (Kriegler et al. 2022) and comparable materials with a low melting point T_m, such as zinc (T_m= 693 °K) (Catalano et al. 2018). Melt formation might be reduced by augmenting the amount of vaporized material through lower wavelengths, elevating lithium metal's laser absorptivity. While lithium metal only absorbs 3 % of laser radiation at λ = 1030 nm, the absorptivity rises to ≈ 9 %, ≈ 15 %, and ≈ 33 % for λ = 515 nm, λ = 450 nm, and λ = 342 nm, respectively (Bocksrocker 2022).

3.2. Lithium metal / copper double-layer

For the lithium metal / copper double-layer, no excessive heat damage was detected for any parameter set, as the copper substrate provides mechanical stability to the lithium layer. The overall lower scan speeds applied resulted in the removal of the lithium layer for most parameter sets. However, complete penetration of the copper substrate was achieved only in a small process window, with the copper foil surface usually exposed along the cutting kerf. In addition, the lithium foil contracted and distorted near the cutting kerf, causing a wave-like surface structure. Both effects are likely due to the differing thermal properties of lithium and copper (Table 1). The low melting point of lithium metal may explain the melt-dominated material removal, even when applying ultrashort laser pulses leading to a reduced heat input (Leitz et al. 2011).

Fig. 7 confirms that high peak pulse fluences are required to ablate the copper foil, indicating a higher ablation threshold for copper than lithium metal. The highest cutting speed of 1.6 m·s^{-1} was achieved at the lowest pulse repetition rate allowing for the highest peak pulse fluence. Elemental maps (compare Fig. 8) revealed copper spatters around the cutting kerf. However, no relevant increase in oxygen contamination was observed, justifying the protective inert gas atmosphere.

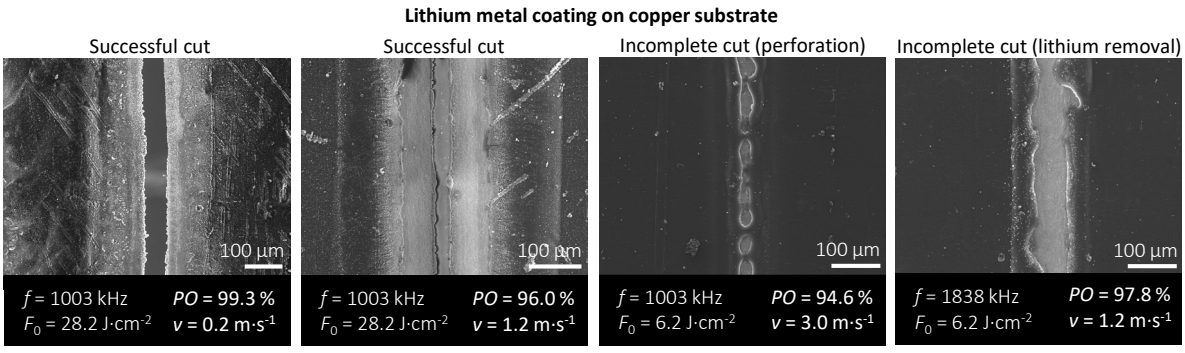

Fig. 6 Scanning electron microscopy images showing successful and incomplete laser cuts in lithium metal / copper double-layers; *f*: pulse repetition rate; *PO*: pulse overlap; F_0: peak pulse fluence, *v*: scanning speed

Table 1. Comparison of physical and thermal properties of lithium and copper at room temperature; references: [a] Davis 2001;[b] Querry 1985; [c] Garrett 2004; [d] Bocksrocker 2022; * values depend on the surface condition

Property	Unit	Copper	Lithium metal
Density ρ	kg·m^{-3}	8930 [a]	534 [c]
Specific heat capacity c_p	kJ·(kg·K)$^{-1}$	0.385 [a]	3.56 [c]
Melting point T_m	K	1358 [a]	454 [c]
Vaporization point T_b	K	2868 [a]	1,616 [c]
Thermal conductivity κ	W·(m K)$^{-1}$	398 [a]	85 [c]
Enthalpy of fusion H_f	kJ·kg^{-1}	205 [a]	432 [c]
Enthalpy of evaporation H_e	kJ·kg^{-1}	4,729 [a]	21,034 [c]
Reflectivity *R* at λ = 1030 nm *	%	≈ 99 [b]	≈ 97 [d]

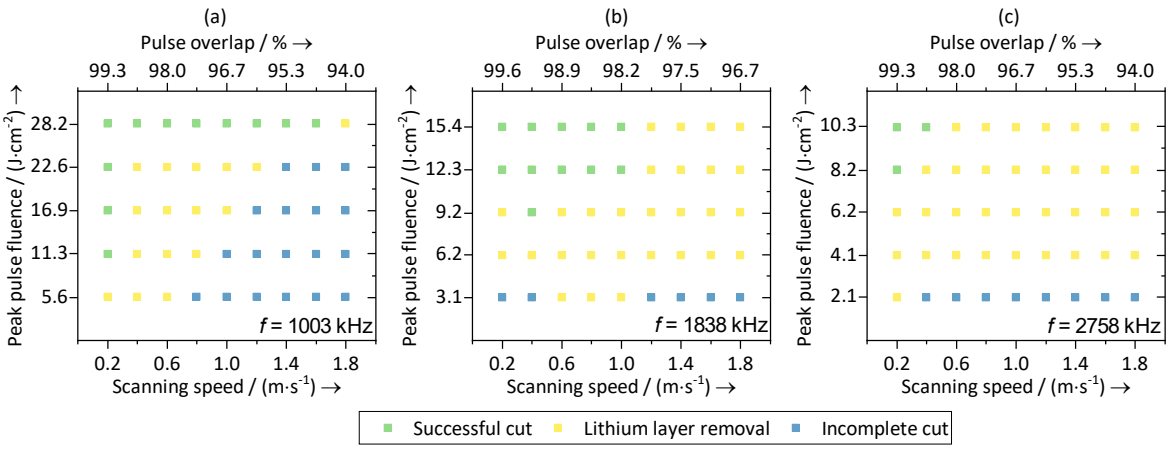

Fig. 7. Parameter windows for laser cutting of lithium metal / copper double-layers at (a) f = 1003 kHz, (b) f = 1838 kHz, and (c) f = 2758 kHz

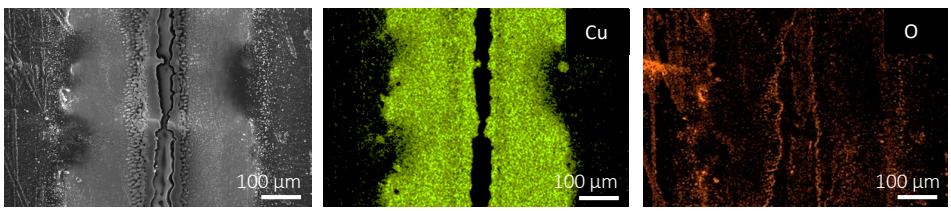

Fig. 8. Scanning microscope image of a lithium metal / copper double-layer cut edge and corresponding elemental maps for copper (Cu) and oxygen (O).

4. Implications for industry

The availability of lithium metal batteries on the market is currently very limited, requiring assumptions about the electrode cut edge length of future battery types to allow for the calculation of process times. Lithium metal battery prototypes have been demonstrated with circumferences around 30 cm (QuantumScape Corporation 2022) and can be expected to be scaled up to the formats of conventional LIBs. For example, the electrode circumference of a Volkswagen ID.3 pouch cell comprises approximately 125 cm (Guenter and Wassiliadis 2022). Fig. 9 depicts the processing times for lithium metal anode cutting as a function of the electrode circumference using the maximum cutting speeds accomplished within this study. The processing time for freestanding lithium metal foil was calculated to be less than 0.5 s, even at an electrode circumference of 200 cm. In contrast, lithium metal / copper double-layers present an increased challenge to achieve the targeted processing times of ≈ 1 s per workpiece known from conventional LIB production.

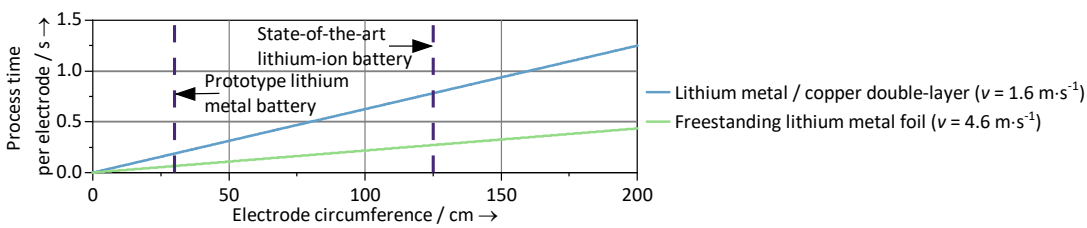

Fig. 9. Process time per electrode as a function of the electrode circumference calculated from the achieved laser cutting speeds within this study for a freestanding lithium metal foil and a lithium metal / copper double-layer foil

5. Conclusion

Within this work, experimental results on picosecond laser cutting of various lithium metal substrates for post-lithium-ion battery production were presented. It was demonstrated that despite applying pulses with durations in the low picosecond regime, the material removal is primarily based on melt expulsion and only subordinately on evaporation. Thus, melt deposition along the cut edge is inevitable, necessitating further considerations of the electrochemical effects induced by these superelevations. It has also been shown that adding a copper current collector foil to the lithium metal anode, forming a double-layer compound, significantly reduces the achievable cutting speed. The different optical and thermal properties of lithium metal and copper were identified as responsible for forming a delamination zone around the cut edge of these substrates.

Future work will investigate ablation cutting of lithium metal anodes using lower pulse overlaps and multiple scan cycles for reducing the melt superelevation. Moreover, shorter laser wavelengths will be tested to extend the portion of evaporation-based material removal for an improved cut edge quality. From an electrochemical perspective, the influence of the chemical composition and the topography of the lithium metal surface around the laser cut edge on battery performance characteristics, such as lithium dendrite formation, needs to be further investigated.

Acknowledgements

This work was financially supported by the German Federal Ministry of Education and Research (BMBF) under the grant number 03XP0184I (ProFeLi). The authors gratefully acknowledge the support. We extend our sincere thanks to IPG Photonics for the provision of the laser beam source used in the experimental studies. Furthermore, the authors thank Prof. Ali Goekhan Demir and his research group for the ongoing professional exchange. The authors take full responsibility for the content of this publication.

References

Andre D, Hain H, Lamp P, Maglia F, Stiaszny B (2017) Future high-energy density anode materials from an automotive application perspective. Journal of Materials Chemistry A 5, p. 17174.

Backlund JR (1977) Method of cutting lithium (4,060,017). https://patents.google.com/patent/US4060017A/en?q=Method+of+cutting+lithium&inventor=backlund&oq=Method+of+cutting+lithium+backlund.

Baumann R, Lasagni AF, Herwig P, Wetzig A, Leyens C, Beyer E (2019) Efficient separation of battery materials using remote laser cutting–high output performance, contour flexibility, and cutting edge quality. Journal of Laser Applications 31, 022210.

Blomgren GE (2017) The Development and Future of Lithium Ion Batteries. Journal of The Electrochemical Society 164, p. A5019–A5025.

Bocksrocker O (2022) Method for processing a lithium foil or a lithium-coated metal foil by a laser beam (US 2022/0234140 A1). Accessed 12 May 2023.

Cano ZP, Banham D, Ye S, Hintennach A, Lu J, Fowler M, Chen Z (2018) Batteries and fuel cells for emerging electric vehicle markets. Nat Energy 3, p. 279.

Catalano G, Demir AG, Furlan V, Previtali B (2018) Prototyping of biodegradable flat stents in pure zinc by laser microcutting and chemical etching. J. Micromech. Microeng. 28, 095016.

Davis JR (2001) Copper and copper alloys. ASM specialty handbook. ASM International, Materials Park OH.

Demir AG, Previtali B (2014) Remote cutting of Li-ion battery electrodes with infrared and green ns-pulsed fibre lasers. The International Journal of Advanced Manufacturing Technology 75, p. 1557.

Duffner F, Kronemeyer N, Tuebke J, Leker J, Winter M, Schmuch R (2021) Post-lithium-ion battery cell production and its compatibility with lithium-ion cell production infrastructure. Nature Energy 6, p. 123.

Garrett DE (2004) Handbook of lithium and natural calcium chloride: Their deposits, processing, uses and properties, 1st edn. Elsevier Acad. Press, Amsterdam.

Genovese M, Louli AJ, Weber R, Hames S, Dahn JR (2018) Measuring the Coulombic Efficiency of Lithium Metal Cycling in Anode-Free Lithium Metal Batteries. Journal of The Electrochemical Society 165, p. A3321.

Guenter FJ, Wassiliadis N (2022) State of the Art of Lithium-Ion Pouch Cells in Automotive Applications: Cell Teardown and Characterization. Journal of The Electrochemical Society.

Ismail I, Noda A, Nishimoto A, Watanabe M (2001) XPS study of lithium surface after contact with lithium-salt doped polymer electrolytes. Electrochimica Acta 46, p. 1595.

Janek J, Zeier WG (2016) A solid future for battery development. Nature Energy 1, 16141.

Jansen T, Blass D, Hartwig S, Dilger K (2018) Processing of Advanced Battery Materials – Laser Cutting of Pure Lithium Metal Foils. Batteries 4, 37.

Krauskopf T, Richter FH, Zeier WG, Janek J (2020) Physicochemical Concepts of the Lithium Metal Anode in Solid-State Batteries. Chem Rev 120, p. 7745.

Kriegler J, Binzer M, Zaeh MF (2021) Process strategies for laser cutting of electrodes in lithium-ion battery production. Journal of Laser Applications 33, 012006.

Kriegler J, Duy Nguyen TM, Tomcic L, Hille L, Grabmann S, Jaimez-Farnham EI, Zaeh MF (2022) Processing of lithium metal for the production of post-lithium-ion batteries using a pulsed nanosecond fiber laser. Results in Materials 15, 100305.

Leitz K-H, Redlingshoefer B, Reg Y, Otto A, Schmidt M (2011) Metal Ablation with Short and Ultrashort Laser Pulses. Physics Procedia 12, p. 230.

Meyer HC (1957) Some Practical Aspects of Handling Lithium Metal. In: American chemical society (ed) Handling and uses of the alkali metals, vol 19, 1155 Sixteenth St., N.W. Washington 6, D.C., p. 9.

Mustafa H, Matthews D, Roemer G (2020) The role of pulse repetition rate on picosecond pulsed laser processing of Zn and Zn-coated steel. Optics & Laser Technology 131, 106408.

Otto S-K, Fuchs T, Moryson Y, Lerch C, Mogwitz B, Sann J, Janek J, Henss A (2021) Storage of Lithium Metal: The Role of the Native Passivation Layer for the Anode Interface Resistance in Solid State Batteries. ACS Appl. Energy Mater. 4, 12798.

Park D, Lee D (2021) Design and Manufacturing of Low Relative Humidity Chamber for Laser Processing of Lithium Metal.

Placke T, Kloepsch R, Duehnen S, Winter M (2017) Lithium ion, lithium metal, and alternative rechargeable battery technologies: the odyssey for high energy density. J Solid State Electrochem 21, p. 1939.

QuantumScape Corporation (2022) White paper: A deep dive into QuantumScape's fast-charging performance. QuantumScape.

Schmitz R, Mueller R, Krueger S, Schmitz RW, Nowak S, Passerini S, Winter M, Schreiner C (2012) Investigation of lithium carbide contamination in battery grade lithium metal. Journal of Power Sources 217, p. 98.

Schmuch R, Wagner R, Hoerpel G, Placke T, Winter M (2018) Performance and cost of materials for lithium-based rechargeable automotive batteries. Nature Energy 3, p. 267.

Schnell J, Guenther T, Knoche T, Vieider C, Koehler L, Just A, Keller M, Passerini S, Reinhart G (2018) All-solid-state lithium-ion and lithium metal batteries – paving the way to large-scale production. Journal of Power Sources 382, p. 160.

Tarascon JM (2010) Is lithium the new gold? Nat Chem 2, p. 510.

Tarascon JM, Armand M (2001) Issues and challenges facing rechargeable lithium batteries. Nature 414, p. 359.

Varzi A, Thanner K, Scipioni R, Di Lecce D, Hassoun J, Doerfler S, Altheus H, Kaskel S, Prehal C, Freunberger SA (2020) Current status and future perspectives of lithium metal batteries. Journal of Power Sources 480, 228803.

Weber DA (2019) Coating for a tool for handling lithium metal, tool and method for producing such a tool (WO2019/162314 Al). https://patentscope.wipo.int/search/en/detail.jsf?docId=WO2019162314.

Wu F, Yuan Y-X, Cheng X-B, Bai Y, Li Y, Wu C, Zhang Q (2018) Perspectives for restraining harsh lithium dendrite growth: Towards robust lithium metal anodes. Energy Storage Materials 15, p. 148.

Wu B, Yang Y, Liu D, Niu C, Gross M, Seymour L, Lee H, Le PML, Vo TD, Deng ZD, Dufek EJ, Whittingham MS, Liu J, Xiao J (2019) Good Practices for Rechargeable Lithium Metal Batteries. Journal of The Electrochemical Society, p. 4141.

Zhang Y, Li J, Yang R, Liu T, Yan Y (2019) Analysis of kerf quality on ultrafast laser cutting of anode material for lithium-ion battery. Optics and Lasers in Engineering 118, p. 14.